

A Study of Relation Between Permeabilities and Pore Space Based on Dilation Operation

Li Daolun¹, Lu Detang¹ and Liu Cong¹

Abstract: CO₂ or acidic material injection into oil reservoirs or Alkaline-surfactant-polymer (ASP) flooding induces reactivity between CO₂, acid, ASP, pore-waters and minerals, which results in modification of porosities and permeabilities. We use dilation operation to simulate the modification of the porosities and study the variation of permeabilities. Firstly we get digital images from CT experiment of a real rock core. Secondly the pore space of digital cores is expanded by dilation operation which is one of basic mathematical morphologies. Thirdly, the distribution of pore bodies and pore throats are obtained from the pore network modeling extracted by maximal ball method. Finally, the relation between network modeling parameters and permeabilities is analyzed.

The result is that the throat change influences the permeability exponentially and that permeabilities are significantly influenced by the big throats.

Keywords: permeability, modification of pore space, dilation operation, pore network model, microscopic percolation.

1 Introduction

Concerns over greenhouse gas emissions are leading to the investigation and realization of carbon storage in recent years. The capture and geological storage of CO₂ is a viable strategy to reduce the release of greenhouse gases to the atmosphere.

CO₂ injection into oil reservoirs has been widely accepted as an effective technique for enhanced oil recovery (EOR), and has been used by the oil industry for over many years [Jessen, Kovscek and Orr (2005)]. The injection of CO₂ into the deep oil reservoirs will result in chemical disequilibria and the initiation of various chemical reactions [Czernichowski-Lauriol, Rochelle, Gaus, Azaroual, Pearce and Durst (2006)]. All the mineralogical reactions are highly complex. They result in

¹ Department of Modern Mechanics, Key Laboratory of Software in Computing and Communication of Anhui Province, University of Science and Technology of China, Hefei 230027, China.

modification of porosities and permeabilities, which influence the actual injection and migration of CO_2 .

To improve oil recovery in the old reservoirs after flooded by water, alkaline-surfactant-polymer (ASP) is injected into oil reservoir as an instead of water. Many chemical reactions exist during ASP flooding, which lead to retention and changes the pore spaces. The retention mechanisms is complex, for an example, Polymer retention depends on many factors such as polymer type, molecular weight, rock composition, brine salinity flow rate [Mantilla and Srinivasan (2011)]. The retention also results in modification of porosities and permeabilities.

Although the length-scale of an oil field is measured in kilometers, the ultimate success of an oil recovery scheme is the result of countless displacement events at a micron-sized scale. The advances in micro-imaging of natural rocks, combined with advances in pore-network modeling, allow researchers to gain a better understanding of pore-level displacement mechanisms.

In this paper we are not involved in the mechanism of these reactions, while investigate the relationship between modification of pore spaces and the permeabilities and how the modification of pore space to influence the flow ability from the pore level.

Microscopic percolation flow is research of porosity media on pore-scale mainly by experimental simulation and numerical simulation [Guang et al. (1990); Bakke (1997); Blunt, Jackson, Piri et al. (2002); Blunt and King (1990); Liang, Fernandes, Magnani and Philippi (1998); Lindquist, Lee, Coker, Jones and Spanne (1996); Al-Kharusi and Blunt (2007); Dong and Blunt (2009); Silin and Patzek (2006)]. By using CT experiment of real core with X-ray, the three-dimensional volume data of rock are acquired with the micron resolution. The microscopic structure of the pore space can be obtained using the algorithm of pore-network modeling from the volume data. In the pore network model, pore bodies represent the spacious part of pore space and throats represent the long-narrow part of pore space. Various characteristics can be predicted during flow of fluids based on the pore network model [Dixit, McDougall and Sorbie (1998); Hazlett (1997); Blunt, Jackson, Piri and Valvatne (2002); Øren and Bakke (2002)].

There are many methods to reconstruct the pore network. The major methods include the medial axis based method and maximal ball method. Medial axis method use image processing to subtract the medial axis to represent the topological skeleton of pore space [Liang, Fernandes, Magnani and Philippi (1998); Lindquist, Lee, Coker, Jones and Spanne (1996)]. The maximal ball [Al-Kharusi and Blunt (2007); Dong and Blunt (2009); Silin and Patzek (2006)] method finds the largest spheres centered on each voxel in the pore space. Maximal method first is proposed by

Silin et al, then extended by Donghu and Blunt. The method of the pore network modeling used in this paper is also extended from maximal ball method the detail of which is in another paper¹. Apart from the direct method to get 3D volume data, there are many indirect ways to generate the pore space, such as the statistical model [Strebelle (2002); Okabe and Blunt (2005); Zhang, Li, Lu and Yang (2010)] and process stimulating method [Øren and Bakke (2002)].

In this article, we first do CT experiment of nature core and get 118 slices of digital images with the 10-micron resolution. Dilation operation, one of basic mathematical morphologies, is used to simulate the increasing of porosity when acidic fluid is injected into oil reservoir. At last, we calculate the permeability of every digital core by Lattice-Boltzman and analyze on the relationship between model parameters and the permeabilities.

2 Core's CT experiment and image processing

2.1 The principle and device of CT experiment

CT experiment is based on the interaction between ray and sample. Different substance in the sample has different absorption coefficient. When ray passes through some substance, its intensity can be expressed by:

$$I = I_0 e^{-\sum u_i D_i} \quad (1)$$

Where u_i is decline coefficient of different substance, D_i is thickness of substance. Because the different absorption coefficient of pore and frame in porous media, we can get the inner structure of core by CT experiment.

We get projection drawing of different angle, the projection data of different angle can be expressed by:

$$p_\phi(x_r) = \int_L u(x,y) dl = \ln(I_{0\phi}(x_r)/I_\phi(x_r)) \quad (2)$$

Where ϕ is projection angle, X_r is coordinates of ray, L is path of ray's pass through sample. The projection data can be calculated by formula (2), then use CT reconstruction algorithm to calculate $u(x,y)$.

In this paper, our experiment utilizes the CT experiment device in Beijing Synchrotron Radiation Facility (BSRF). The light source is X-ray, scanner system gets one projection image every one degree. The image collection system uses CCD whose resolution is 10um. The experimental sample is a cylindrical sandstone core whose diameter is 3mm.

¹ Will be published in "Petroleum Science and Technology"

2.2 Image processing

The original images obtained from CT experiment are grayscale image and need to image processing. After noise removal, image enhancement and image segmentation, the grayscale images is turned into binary images, in which each voxel is represented by a single bit, being 1 for pore and 0 for solid (see Figure 1).

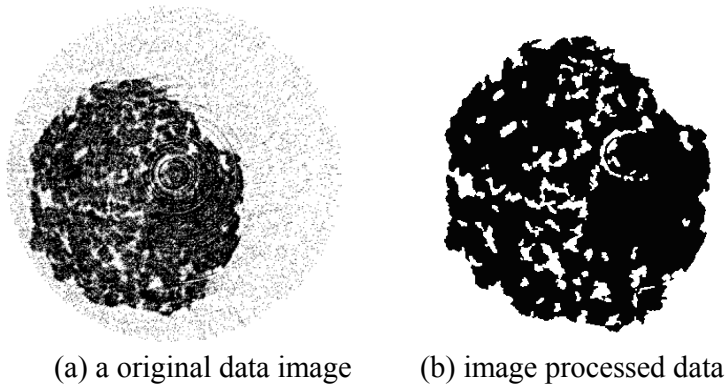


Figure 1: Image Processing.

It is either costly or unavailable to obtain the experimental data of a rock before and after flooding by CO₂, ASP or acidic fluid at the millimeter-sized scale. Therefore the digital image processing technique is used to approximately simulate the change of pore space caused by the chemical reaction.

2.3 Basic morphological operations: erosion and dilation

The basic morphological operations, erosion and dilation, can change the size of objects when applied to either grayscale or binary images. Erosion shrinks image objects while dilation expands them.

The characteristics of erosion are that erosion generally decreases the sizes of objects and removes small anomalies by subtracting objects with a radius smaller than the structuring element. So erosion is used to stimulate the decrease of the pore space.

On the contrary, the characteristic of dilation is that dilation generally increases the sizes of objects. With binary images, dilation adds pixels to the perimeter of each image object. So erosion is used to stimulate the increase of the pore space.

The number of pixels added or removed from the objects in an image depends on the size and shape of the structuring element used to process the image. A

structuring element is a matrix consisting of only 0's and 1's that can have any arbitrary shape and size.

Two-dimensional structuring elements are typically much smaller than the image being processed. A square structuring element used in this paper is a 2×2 matrix:

$$\mathbf{P} = \begin{bmatrix} 1 & 1 \\ 1 & 1 \end{bmatrix}$$

Figure 2 shows the original image (see figure 2 b), the corresponding eroded image (see figure 2 a) and corresponding dilated image (see figure 2 c)

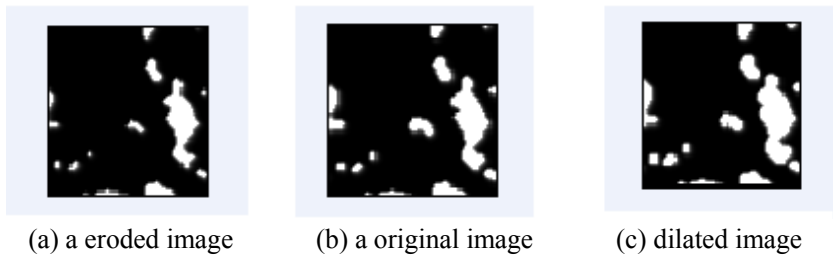


Figure 2: eroded and dilated images, white color represents pore space.

2.4 Three digital cores generated by erosion operation

Erosion shrinks image objects while dilation expands them. In this sense, erosion is contrary to the dilation. So we just use dilation to simulate the modification of pore space.

The whole digital core consists of a huge number of voxels. A simulation with so many voxels based on Lattice-Boltzman would be a challenge for a computer. Therefore only 80 serial binary images of pore space and the $80 \times 80 \times 80$ pixels are combined in a computer to a 3D matrix of voxels represented by single bits.

Three other types of digital cores are generated by the dilation operation based on the original $80 \times 80 \times 80$ digital core. The first type is that the previous 20 serial binary images are dilated while other sixty images are not, which is marked as “20d”. The second type is that only previous 40 serial binary images are dilated and marked as “40d”. The third type is that only 60 serial binary images are dilated and marked as “60d”. The original image is marked as “0d”.

Intuitively we can know that the porosities and permeabilities increase gradually from “0d” digital cores, “20d” digital cores, “40d” digital cores to “60d” digital

cores. Therefore the process of acidic fluid interact with the solid is approximately simulated.

Table1 gives the porosity of 4 types of digital cores. It shows that the porosity increase linearly from 0.1705 to 0.2050, which is also shown in Figure 5.

Table 1: Distribution of radius of pore body

Sample No	0d	20d	40d	60d
porosity	0.1705	0.1803	0.1915	0.2050

3 Pore network modeling reconstruction method

The pore space of porous media is complex, localized disordered and not a simple geometric body. For simplification the pore space is always replaced by some kind of simple objects. By the same way in this article, we consider the pore body as sphere and the throat as cylinder to construct the pore network modeling.

There are many pore network modeling methods to distinguish between the pore bodies and pore throats, and establishes their respective volume and connectivity. The main idea of the algorithm is introduced below.

In the discrete space the concept of sphere is a little different from the concept of sphere in the continuous space. Figure 3 gives the circle with radius of 1 to radius 3.

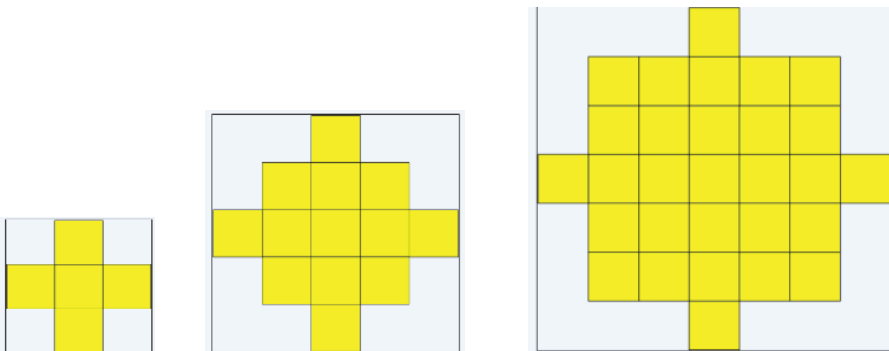


Figure 3: plane view of pore body with different radius (from left to right, $r=1$, $r=2$, $r=3$)

The first step is to divide original pore space into sphere pore bodies which are not included and disjointed by each other, and save the information of each sphere with their center and radius for next step calculation.

The second step is to search and reconstruction of throat. The throat is considered to be a long-narrow space that connects two pore bodies, and it is also the channel in which fluid flow from one pore body to another. The throat can be constructed by searching the connected path between two pore neighboring bodies. The cross section area of throat can be considered as the narrowest area of channel, and will be used to define the radius of the throat.

As the throat is simplified as a cylinder and the section of the cylinder is circle, the radius of throat is calculated by the formula below

$$\pi r^2 = width \quad (3)$$

Where, r is the radius of the circle, and $width$ is the section area of a throat. Because the shape of the throat is very complex, the radius of throats is an approximate value.

4 The reconstruction result

4.1 The distribution of pore body' radius

Import the three dilated and the original digital cores and reconstruct them with pore network model. The distribution of pore body radius could describe spacious space of pore. The reconstruction result of pore body is showed in Table 2.

Table 2: Distribution of radius of pore body

	0d	20d	40d	60d
The number of pore body with radius of 5	3	4	5	8
The number of pore body with radius of 4	25	26	31	38
The number of pore body with radius of 3	21	23	26	29
The number of pore body with radius of 2	394	407	422	418

Table 2 shows that the number of pore bodies with radius of 3, 4 and 5 increases when more images are dilated. It shows that there are more big pore bodies in digital cores with more dilated images. However it is not true for the small pore bodies with radius, for an example, for among pore bodies with radius of 2, "40d" digital core owns the largest number.

The columns of Table 2 show that as the radius of sphere increases the number of sphere pore body decreases dramatically. It shows that most of the space is small pore particle in porous media.

4.2 The distribution of throat radius

After reconstruction of sphere pore body, the pore throats are searched and constructed. The number of throats is statistic according to the discrete versions of the balls, which are shown in Figure 2. The number of pore throats given below is based on discrete version while not based on the continuous version.

The number of throats of different radius is counted as follow:

If the section area of a throat is in the interval [29, 53], the radius of the throat is 3;

If the section area of a throat is in the interval [14, 28], the radius of the throat is 2;

If the section area of a throat is in the interval [5, 13], the radius of the throat is 1;

If the section area of a throat is in the interval [1, 4], the radius of the throat is less than 1, marked as 0.5;

The number of the throats is given in table 3.

Table 3: Distribution of pore throat

	0d	20d	40d	60d
Radius = 3	4	4	5	10
Radius = 2	12	14	17	22
Radius = 1	174	199	202	205
Radius < 1	496	530	537	544

Table 3 shows that when more images are dilated, the radii of throats increase. The “0d” digital core and the “20d” digital core have equal number of pore throats with radius of 3, which means that the largest pore throat does not exit in previous 20 images.

The distribution of the number of throats with different radii is also shown in Figure 4, which apparently shows that the number of throat decrease greatly when the radius of throat increases.

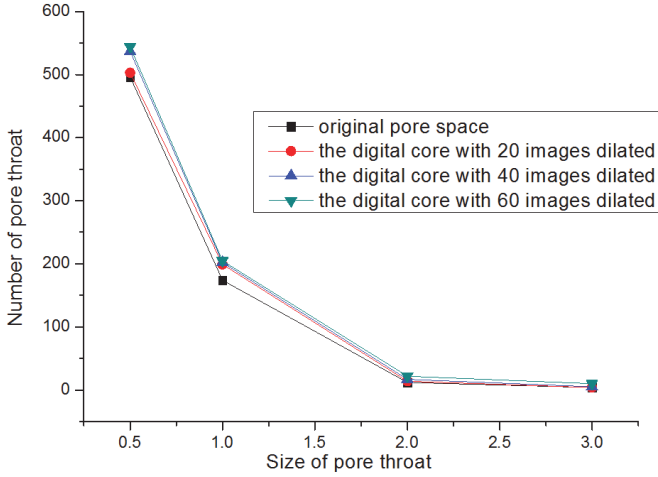


Figure 4: Distribution of throat.

5 Permeability calculation and analysis

5.1 Permeability calculation with LBM method

There are two types model to simulate flow in porosity media at pore scale. One is network flow modeling and the other is Lattice-Boltzman. In this paper, we use Lattice-Boltzman to simulate flow and calculate the absolute permeability of four digital core samples in order to analysis the relationship between network model parameters and permeabilities. Here D3Q19 model ^[20] is used and its evolution equation is:

$$f_i(x + \Delta x, t + \Delta t) = f_i(x, t) - \frac{1}{\tau}(f_i(x, t) - f_i^{eq}(x, t)) \quad (4)$$

Where $f_i(x, t)$ is distribution function at time t , location x and direction i . $f_i^{eq}(x, t)$ is equilibrium distribution function, it can be described as:

$$f_i^{eq}(x, t) = w_i \rho \left[1 + 3 \frac{e_i \cdot u}{c^2} + 4.5 \frac{(e_i \cdot u)^2}{c^4} - 1.5 \frac{u^2}{c^2} \right] \quad (5)$$

w_i is weight value, e_i is discrete velocity. They can be expressed as follows:

$$w_i = \begin{cases} 1/3 & i = 0 \\ 1/18 & i = 1, 2, \dots, 6 \\ 1/36 & i = 7, \dots, 18 \end{cases} \quad (6)$$

$$e_i = \begin{cases} (0,0,0) & i = 0 \\ (\pm 1, 0, 0), (0, \pm 1, 0), (0, 0, \pm 1) & i = 1, 2, \dots, 6 \\ (\pm 1, \pm 1, 0), (\pm 1, 0, \pm 1), (0, \pm 1, \pm 1), & i = 7, \dots, 18 \end{cases} \quad (7)$$

The density and momentum of fluid can be expressed by:

$$\rho = \sum f_i(x, t) \quad (8)$$

$$\rho u = \sum f_i(x, t) e_i \quad (9)$$

5.2 The relationship between permeabilities and other porous media parameters

There are many porosity media parameters such as porosity, coordination number, the distribution of pore body and throat. The coordination number of a pore body is the number of pore throats connecting it to other pore bodies. It is one of important parameters of pore space because the connections of pore throat control the flow properties. Since the four types of the digital core almost have the same morphologies, the analysis of coordination number is neglected.

As definition of pore network model, a complete flow channel consists of two elements, pore body and throat. Pore throats are the narrow gateways that connect the pore bodies and determine the rock permeabilities. The pore body is spacious pore space for storing fluid. Generally, pore bodies determine the rock porosity. Therefore the analysis of the relation between permeabilities and pore bodies is omitted.

5.3 The relationship between permeabilities and porosities

The permeability is calculated by above mentioned LBM method. In order to observe the effect of porosity to permeability, we sort the four samples according to their porosity from low to high. The order is “0d” digital core, “20d” digital core, “40d” digital core, “60d” digital core, shown as Figure 5.

As is showed in Figure 5, permeabilities go up as porosities increase. Although the increasing trend is same, the increasing rates have a big difference. The porosity increases linearly while the permeability increases exponentially. It shows that the porosity is not the main influencing factors to the permeability.

5.4 The distribution of throat radius

The permeabilities and the number of throats for all samples are shown in Figure 6, where the number of throats with radius of 1 is minus 150 for displaying conveniently. It is easy to see that there is big difference between distribution of the

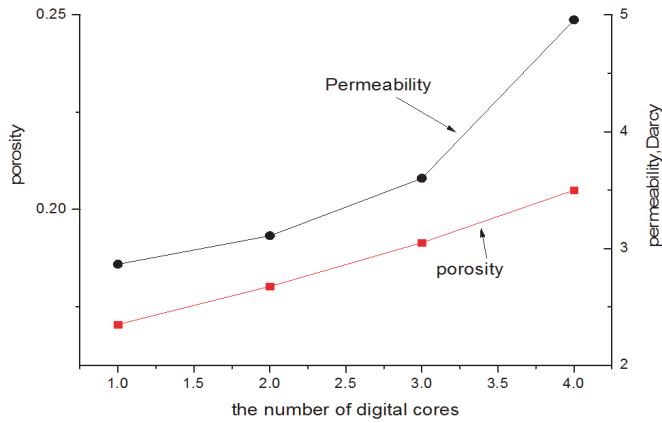


Figure 5: Relationship between the permeabilities and the porosities.

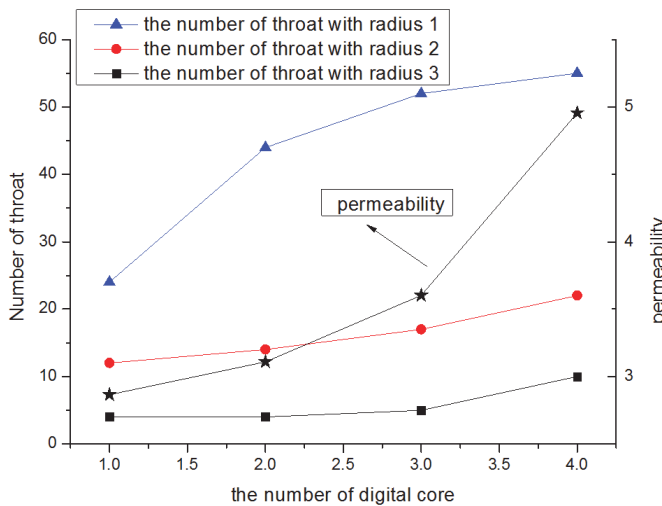


Figure 6: Relationship between permeability and the Number of big throats.

permeability and distribution of the throat with a radius of 1. Their trends are different. Therefore the small pore throats are not essential factor for permeabilities.

Figure 6 shows that the trend of the throats with radii of 2 and 3 more coincides with the distribution of permeabilities. The throats with radii of 2 and 3 are called big throats here, which only have a small proportion of the whole throats.

In order to see the relation between big throats and permeabilities, we add the number of throat with radius of 3 and 2. The big throats and permeabilities are

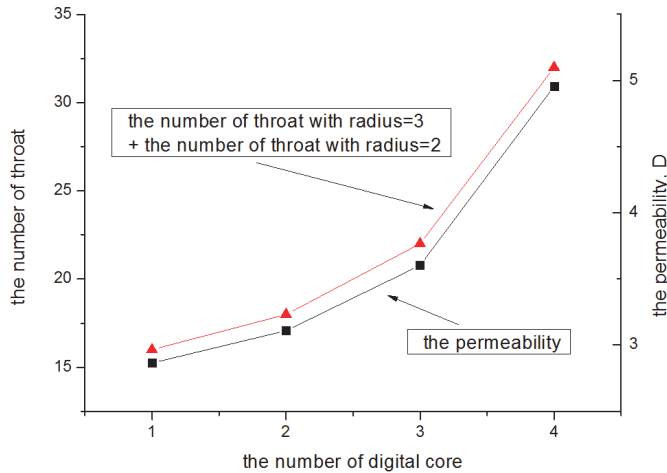


Figure 7: Relationship between the permeability and the number of large pore body.

plotted in Figure 7 at different scale.

Figure 7 gives us a surprising result that the two Line segments are almost parallel to each other although they are shown at different scales. The permeability increases in the same way as the number of big throats increases. It shows that permeability K is significantly influenced by the number of big throats. It can be interpreted by Hagen-Poiseuille formula and the Darcy law.

In pore network model of porous media, the flow channel is composed of many cells of pore body connected by throat. Every channel can be considered as a capillary. As Hagen-Poiseuille formula:

$$Q = (p_i - p_j) \frac{\pi r^4}{8\mu L}$$

From the Darcy law and Hagen-Poiseuille formula, the permeability is mainly decided by r^2 , therefore the big throats decide the value of the permeability.

6 Conclusion

Based on the real data getting from core's CT experiment, we obtain other three samples of digital core with the operation of dilation to simulation the modification of pore space. Their permeabilities are calculated with LBM method.

The other three digital cores origin from a natural rock and the original digital core and other three dilated digital cores have the same topological structure. Therefore,

they have the same distribution of cooperation number and pore bodies. Apart from the influence of the different topological structure, the relation among the permeabilities, porosities and pore throats can be more exactly analyzed.

The result is that the modification of throat changes permeability greatly and that permeability is significantly influenced by the number of big throat. The permeability increases in the same way as the number of big throats increases, although the curves are shown at different scales.

When CO₂, ASP or acid fluid is injected into oil reservoir, the permeability of the rocks will apparently change. From the microstructure of rock, it is interesting that how the velocity, concentration and other factors influence the size of the throats.

Reference

Al-Kharusi, A. S.; Blunt, M. J. (2007): Network extraction from sandstone and carbonate pore space images.

Bakke, A.; Øren, P. E. (1997): 3-d pore-scale modeling of sandstones and flow simulations in the pore networks. SPE 35479, 1997.

Blunt, M. J.; Jackson, M. D.; Piri, M. et al. (2002): Detailed physics, predictive capabilities and macroscopic consequences for pore-network models of multiphase flow. *Adv Water Res*, vol. 25, pp. 1069-1089.

Blunt, M.; King, P. (1990): Macroscopic parameters from simulations of pore scale flow. *Physical Review A*, vol. 42, no. 8, pp. 4780-4787.

Blunt, M. J.; Jackson, M. D.; Piri, M.; Valvatne, P. H. (2002): Detailed physics predictive capabilities and macroscopic consequences for pore-network models of multiphase flow. *Advances in Water Resources*, vol. 25, no. 1, pp. 1069-1089.

Czernichowski-Lauriol, I.; Rochelle, C.; Gaus, I.; Azaroual, M.; Pearce, J.; Durst, P. (2006): Geochemical interactions between CO₂, pore-waters and reservoir rocks. *Earth and Environmental Sciences*, vol. 65, PART III, pp. 157-174.

Dixit, A. B.; McDougall, S. R. (1998): Sorbie K S.A pore-level investigation of relative-permeability hysteresis in water-wet systems. *SPE J.*, vol. 3, no. 2, pp.115-123.

Dong, H.; Blunt, M. J. (2009): Pore-network extraction from micro-computerized-tomography images. *Physical Review E*, vol. 80, pp. 036307.

Guang, S. et al. (1990): *The physical and chemistry mechanism of microcosmic percolation flow*. Beijing: Science Press,1990, pp. 6-18.

Hazlett, R. D. Statistical characterization and stochastic modeling of pore networks in relation to fluid flow. *Mathematical Geology*, vol. 29, no. 4, pp. 801-822.

Jessen, K.; Kovsky, A. R.; Orr, F. M. (2005): Increasing CO₂ storage in oil recovery. *Energy Conversion and Management*, vol. 46, no. 2, pp. 293-311.

Liang, Z. R.; Fernandes, C. P.; Magnani, F. S.; Philippi, P. C. (1998): A reconstruction technique for three-dimensional porous media using image analysis and Fourier transforms. *Journal of Petroleum Science and Engineering*, vol. 21, pp. 273.

Lindquist, W. B.; Lee, S. M.; Coker, D.; Jones, K.; Spanne, P. (1996): Medial axis analysis of void structure in three-dimensional tomographic images of porous media. *J. Geophys. Res.*, vol. 101B, pp. 8297-8310.

Mantilla, C.; Srinivasan, S. (2011): Feedback Control of Polymer Flooding Process Considering Geologic Uncertainty, spe 141962, 2011.

Okabe, H.; Blunt, M. J. (2005): Pore space reconstruction using multiple-point statistics. *Journal of Petroleum Science and Engineering*, vol. 46, pp. 121– 137.

Øren, P. E.; Bakke, S. (2002): Process based reconstruction of sandstones and predictions of transport properties. *Transport in Porous Media*, vol. 46, no. 2, pp. 311-343.

Robert, S. M.; Robert, S. B.; Daryl, W. G. (1996): Boundary conditions for the lattice boltzmann method. *Phys Fluids*, vol. 8, no. 7, pp. 1788—1800.

Silin, D. B.; Patzek, T. W. (2006): Pore space morphology analysis using maximal inscribed spheres. *Physica A*, vol. 371, pp. 336–360.

Strebelle, S. (2002): Conditional simulation of complex geological structures using multiple-point statistics. *Mathematical Geology*, vol. 34, no. 1, pp. 1-21.

Zhang, T.; Li, D.; Lu, D.; Yang, J. (2010): Research on the reconstruction method of porous media using multiple-point geostatistics. *Science in China Series G: Physics, Mechanics & Astronomy*, vol. 53, no. 1, pp. 122-134.